before fixation. Wandering third instar female larval imaginal discs were dissected, fixed, blocked, incubated with antibodies, washed and mounted as described in J. Kim *et al*., *Cell* **82**, 795 (1995). Antibodies and the dilutions at which they were used were: rabbit antibody against β-galactosidase (Cappel or Molecular Probes; 1:500 or 1:1000); mouse antibody against MYC (provided by S. Blair; 1:4); rabbit antibody against MYC (Santa Cruz Biotechnology; 1:200); rabbit antibody against WG (provided by S. Cumberledge; 1:1000); mouse anti body against CUT (Developmental Studies Hybridoma Bank; 1:4). X-gal staining was performed as described [Y. Hiromi, W. J. Gehring, *Cell* **50**, 963 (1987)].

15. The *cut* 0.7-kb cis-regulatory element is the 0.7 kb at the 3′ end of the *cut* gene wing margin enhancer (*12*), which drives reporter gene expression along the presumptive wing margin. The *sal* 328-bp enhancer is a subfragment of the *sal* 10.2-kb enhancer (*13*), that drives expression in a wing pouch-restricted, albeit altered, pattern. Reporter constructs were made by cloning polymerase chain reaction (PCR)–generated fragments of the *cut* gene wing margin or *sal* enhancers into the Hsp *lac*Z-CaSpeR plasmid [H. Nelson, A. Laughon, *Roux's Arch. Dev. Biol.* **202**, 341 (1993)]. The GenBank accession numbers for the *cut* 0.7-kb and *sal* 328-bp cis-regulatory elements are AF369916 and AF369917, respectively.
16. Generation of the SD TEA domain, DNase I footprinting, and electrophoretic mobility-shift assays were performed as described (*7*). Probes for footprinting were generated by end-filling subfragments of cis-regulatory elements with radioactively labeled nucleotides. Probes for shifts were annealed oligonucleotides that were radioactively labeled by kinase or end-filling with Klenow. Sequences protected by the SD TEA domain were aligned and analyzed using the PileUp program of GCG [Wisconsin Package Version 9.1, Genetics Computer Group (GCG), Madison, WI], with adjustments by hand.
17. Sequences of the upper strand of oligonucleotides used as probes for shifts and as PCR primers to mutate SD-binding sites (positions noted in parentheses) in the various cis-regulatory elements are listed in the 5′ to 3′ orientation. Altered bases are shown in lowercase in the mutant version, and the corresponding bases are underlined in the native sequence. At least three independent transgenic lines were analyzed for each set of SD sites mutated.
sal (126) wild type:
5′ TTAAAGATGCTTTCTGGAATCCCACGAATGTCC-ATTGGATGG 3′
sal (126) mutant:
5′ TTAAAGATGCTTTCTctAATCagACtAATGaggATTGG-ATGG 3′
cut (558) wild type:
5′ TTTGTCAATGTAATTCGAAAAATGTCGTCAG 3′
cut (558) mutant:
5′ TTTGTCAATcTAATTCtActAATtTCGTCAG 3′
vgQ 1 (87) wild type:
5′ GCGTTGACAACATTCCAAACTCG 3′
vgQ 1 (87) mutant:
5′ GCGTTGACAtgAgctCttACTCG 3′
vgQ 2 (359) wild type:
5′ ATACGGGATGCCATGCCGCGTGC 3′
vgQ 2 (359) mutant:
5′ ATACGGGATctCATGagGCGTGC 3′
vgQ 3 (450) wild type:
5′ GAGGCCGTGGAATTCCCATTAATG 3′
vgQ 3 (450) mutant:
5′ GAGGCCGTctAATTagCATTAATG 3′
vgQ 4 (488) wild type:
5′ CTGCCAAAGATATTTCCTCTGCAG 3′
vgQ 4 (488) mutant:
5′ CTGCCAAActTATTTCCTCTGCAG 3′
18. X. Liu, M. Grammont, K. D. Irvine, *Dev. Biol.* **228**, 287 (2000).
19. de J. Celis, A. Garcia-Bellido, S. Bray, *Development* **122**, 359 (1996).
20. C. Neumann, S. Cohen, *Development* **122**, 3477 (1996).
21. C. Micchelli, E. Rulifson, S. Blair, *Development* **124**, 1485 (1997).
22. J. de Celis, R. Barrio, F. Kafatos, *Nature* **381**, 421 (1996).
23. M. Zecca, K. Basler, G. Struhl, *Cell* **87**, 833 (1996).
24. J. Kim, K. Johnson, S. B. Carroll, A. Laughon, *Nature* **388**, 304 (1997).
25. C. J. Neumann, S. M. Cohen, *Development* **124**, 871 (1997).
26. K. Certel, A. Hudson, S. B. Carroll, W. A. Johnson, *Development* **127**, 3173 (2000).
27. A. M. Bailey, J. W. Posakony, *Genes Dev.* **9**, 2609 (1995).
28. J. B. Hudson, S. D. Podos, K. Keith, S. L. Simpson, E. L. Ferguson, *Development* **125**, 1407 (1998).
29. D. T. Nellesen, E. C. Lai, J. W. Posakony, *Dev. Biol.* **213**, 33 (1999).
30. Synthetic regulatory elements were constructed by ligating annealed oligonucleotide pairs encoding paired transcription factor–binding sites into the Eco RI and Asp^{718} sites of Hsp *lac*Z-CaSpeR. Each construct consisted of an "A" and a "B" set of annealed oligonucleotides joined with a Bgl II site. The sequences of the top strand for each of the oligonucleotide pairs are as follows, listed in the 5′ to 3′ orientation: $[SD]_2$-A, aattcccaAACTATGCcAGGAATTaaaa; $[SD]_2$-B, gatctccaAACTATGCcAGGAATTaaagaattcg; $[SU(H)]_2$-A, aattGTTCTCACGgatccaaagGTTCTCACGa; $[SU(H)]_2$-B, gatctGTTCTCACGgatccaaagGTTCTCACGgaattcg; [MADMED]-A, aattGCCGTCGCgattcgacaactttGGCCGGCa; [MADMED]-B, gatctGCCGTCGCgattcgacaactttGGCCGGCgaattcg. The transcription factor–binding sites within each oligonucleotide are capitalized; linker sequences are in lower case. In each of the signal and selector constructs the annealed 5′ signal oligonucleotide pair (A) was ligated to the 3′ selector oligonucleotide pair (B). In signal alone or selector alone constructs, the 5′ and 3′ pairs of the appropriate sites were ligated to one another. Wing disc-specific reporter expression was observed in 6 out of 8 lines for $[SU(H)]_2$ $[SD]_2$; 3 out of 7 lines for $[MADMED]_2$ $[SD]_2$; 1 out of 17 lines for $[SU(H)]_2$; 1 out of 17 lines for $[MADMED]_2$; and 1 out of 15 lines for $[SD]_2$.
31. J. Williams, S. Paddock, K. Vorwerk, S. Carroll, *Nature* **368**, 299 (1994).
32. D. Nellen, R. Burke, G. Struhl, K. Basler, *Cell* **85**, 357 (1996).
33. T. Lecuit, W. Brook, M. Ng, M. Calleja, H. Sun, S. Cohen, *Nature* **381**, 387 (1996).
34. R. D. Kornberg, *Trends Cell Biol.* **9**, M46 (1999).
35. H. R. Goodman, S. Smolik, *Genes Dev.* **14**, 1553 (2000).
36. SD binds to discrete domains of CBP in vitro but does not interact with MAD or SU(H) (C. E. Nelson, S. B. Carroll, unpublished observations).
37. N. C. Grieder, T. Marty, H.-D. Ryoo, R. S. Mann, M. Affolter, *EMBO J.* **16**, 7402 (1997).
38. We thank D. Nellen for identifying and providing the *sal* 328-bp element and transgenic flies;. S. Blair, K. Irvine, R. Schuh, and J. Jack for providing fruit fly stocks; T. Stone and J. Posakony for SU(H) protein; A. Laughon for MAD protein and probes; D. Dorsett for *cut* sequence and DNA; V. Kassner, J. Selegue, and K. Vacarro for invaluable technical assistance; L. Olds for figure preparation; J. Carroll for manuscript preparation; M. Levine for helpful discussion; and A. Kopp, G. Panganiban, and T. Wittkopp for comments on the manuscript. J. Magee initiated the studies of SD site mutations in the *vg* Q enhancer, and J.-Y. Sgro and the Institute for Molecular Virology provided access to GCG. Supported by NIH postdoctoral fellowships to K.A.G. and M.E.K., and the Howard Hughes Medical Institute, of which S.B.C. is an Investigator.

14 December 2000; accepted 20 March 2001
Published online 12 April 2001;
10.1126/science.1058312
Include this information when citing this paper.

Physical Properties Determining Self-Organization of Motors and Microtubules

Thomas Surrey,* François Nédélec,* Stanislas Leibler,† Eric Karsenti‡

In eukaryotic cells, microtubules and their associated motor proteins can be organized into various large-scale patterns. Using a simplified experimental system combined with computer simulations, we examined how the concentrations and kinetic parameters of the motors contribute to their collective behavior. We observed self-organization of generic steady-state structures such as asters, vortices, and a network of interconnected poles. We identified parameter combinations that determine the generation of each of these structures. In general, this approach may become useful for correlating the morphogenetic phenomena taking place in a biological system with the biophysical characteristics of its constituents.

A central question in biology concerns the origin of complex macroscopic structures. Two fundamentally different mechanisms can account for the generation of large-scale structures from random mixtures of small molecules. One mechanism is self-assembly near thermodynamic equilibrium (*1*, *2*). A very different mechanism is self-organization in energy-dissipating systems. Although they do not reach thermodynamic equilibrium, these systems can reach steady states; kinetic parameters can influence or determine the final structures (*3*, *4*). In eukaryotic cells, organization of the intracellular architecture is largely determined by the collective behavior of the ensemble of proteins that constitute the cytoskeleton (*5*, *6*). A remarkable property of the cytoskeleton resides in the versatility of all patterns that can be produced. Indeed, similar sets of components are found to be organized into very different assem-

Cell Biology and Biophysics Program, European Molecular Biology Laboratory, 69117 Heidelberg, Germany.

*These authors contributed equally to this work.
†Present address: Departments of Physics and Molecular Biology, Princeton University, Princeton, NJ 08544, USA.
‡To whom correspondence should be addressed. E-mail: karsenti@embl-heidelberg.de

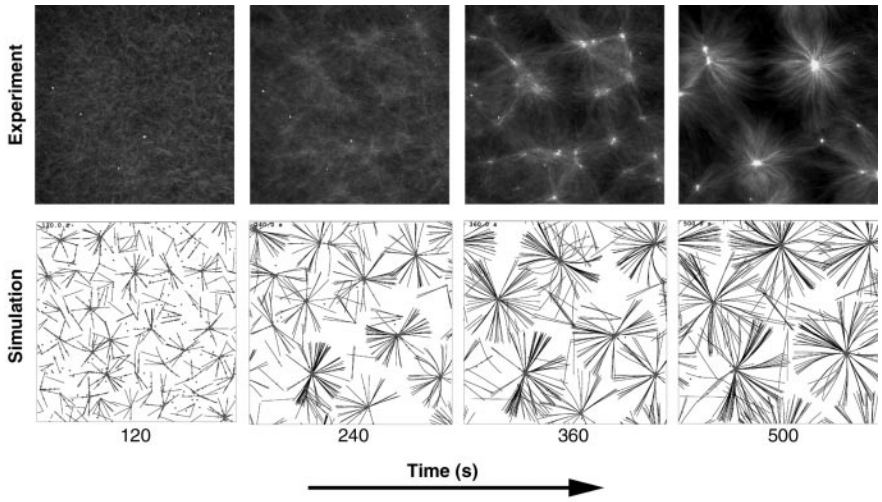

Fig. 1. Kinetics of aster formation by multimeric kinesin complexes as observed in vitro by dark-field microscopy or as reproduced in numerical computer simulations. Experimental conditions are as in Fig. 2, and simulation parameters as in Fig. 3.

blies, depending on the cell type and cell cycle stage. Motor proteins and filaments play an important role in determining the final structure (*7–9*). How their concentrations and the combination of plus- and minus-end motors contribute to morphogenetic processes is not understood. Moreover, other parameters like the speed of different motors, their processivity, or the time they spend bound at microtubule (MT) ends may strongly influence the patterns generated at steady state.

Here, we analyzed the contribution of multiple parameters to the formation of steady-state patterns generated by MTs and soluble motor complexes. Plus-end motors and MTs can self-organize and create structures such as vortices and asters when these motors are multimeric (*10*). The structures emerge within 10 to 20 min after the addition of kinesin complexes to purified tubulin in the presence of adenosine 5′-triphosphate

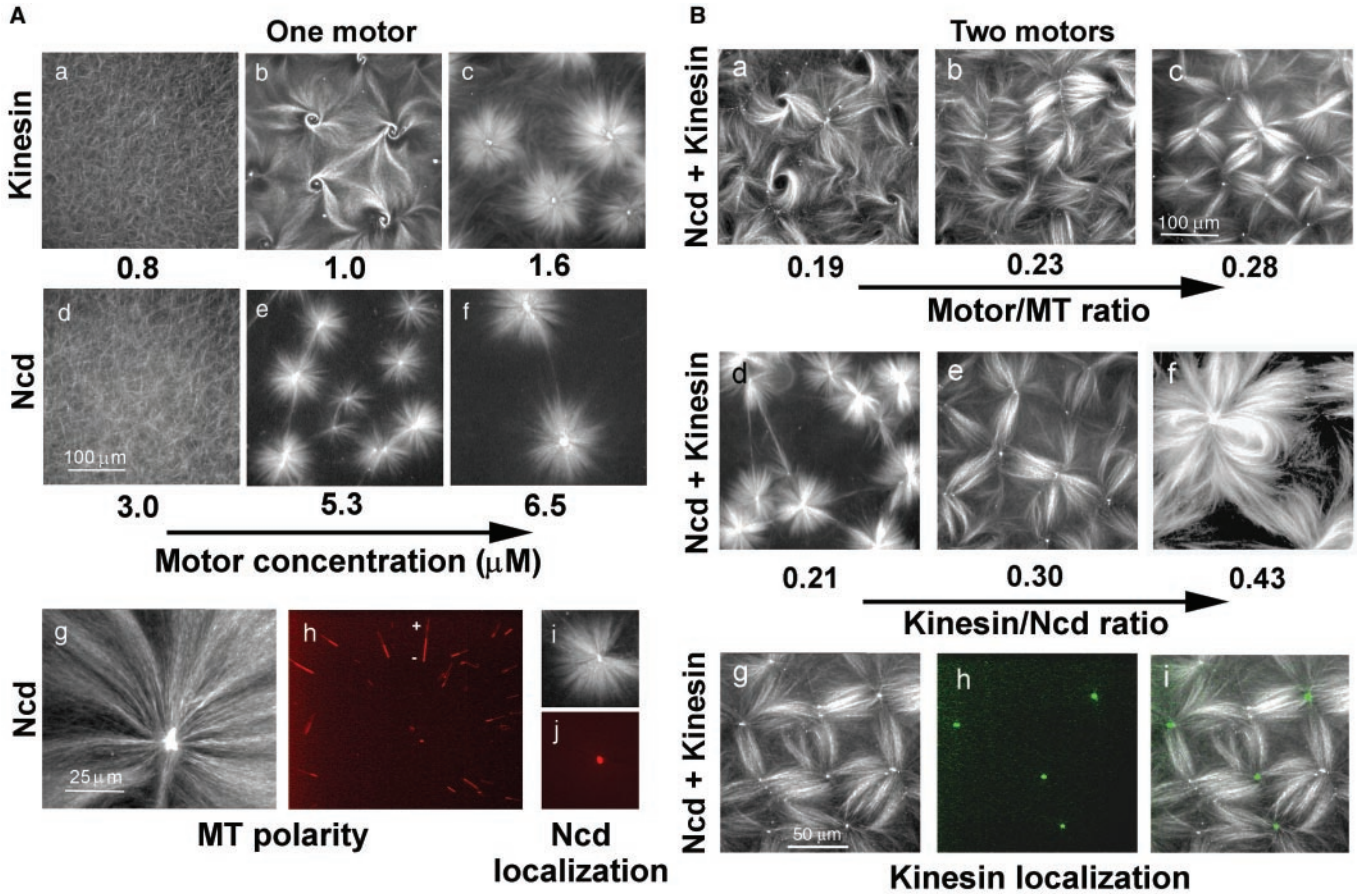

Fig. 2. MT patterns organized in vitro by the action of multimeric motor complexes. (**A**) One species of motor complex: Variation of the concentration of multimeric kinesin complexes (a to c) and of multimeric Ncd complexes (d to f). MTs are visualized by dark-field microscopy. The concentrations of the monomeric motors are indicated. The kinesin (monomer)/streptavidin (tetramer) ratio was maintained at 16, and the GST-Ncd (monomer)/anti-GST ratio at 5.3. Tubulin concentrations were 26 μM in kinesin experiments (a to c) and 23 μM in Ncd experiments (d to f). MT orientation in Ncd asters is shown with tetramethylrhodamine-labeled polarity-marked MT seeds (g: darkfield, h: fluorescence). The bright part of the seeds indicates the minus end. Motor localization is shown in asters organized by tetramethylrhodamine-labeled Ncd complexes (i: dark-field, j: fluorescence). (**B**) Simultaneous action of multimeric kinesin and multimeric Ncd: Variation of the motor/tubulin ratio (without changing the Ncd/kinesin ratio) (a to c). The concentrations of kinesin, Ncd, and tubulin were 1.2, 4.0, and 28 μM (a); 1.5, 4.9, and 28 μM (b); and 1.7, 5.6, and 26 μM (c), respectively. Variation of the kinesin/Ncd concentration ratio (d to f). Kinesin and Ncd concentrations were 1.2 and 5.6 μM (d), 1.7 and 5.6 μM (e), and 2.0 and 4.6 μM (f), respectively. The tubulin concentration was 28 μM. The localization of kinesin in MT networks is shown with the use of fluorescein-labeled kinesin (g: dark-field, h: fluorescence, i: overlay; conditions as in c). Images were taken 10 to 20 min (A) or 25 to 30 min (B) after the start of MT polymerization. For methods, see (*12*, *28*).

(ATP) and guanosine 5′-triphosphate (GTP) (Fig. 1). As an example of a multimeric minus-end motor, we prepared a complex of glutathione-S-transferase–nonclaret disjunctional (GST-Ncd) fusion proteins (*11*) bound to antibodies to GST (anti-GST) and compared directly the effect of the oligomeric kinesin and Ncd constructs on MT organization (Fig. 2A) (*12*). At low motor concentrations, MTs remained randomly oriented. When the concentration was increased, kinesin formed MT vortices at intermediate concentration and asters at higher concentration. Vortices and asters appear to be true steady-state structures (*13*). At no time did we observe the transformation of a vortex into an aster. In contrast to kinesin, Ncd did not form vortices at any of the concentrations tested. As soon as the Ncd concentration was high enough to organize MTs, asters formed. Asters organized by Ncd or kinesin looked similar, but the MT orientation was different. In Ncd-organized asters, the minus ends of the MTs pointed toward the center (as revealed by the orientation of added MT seeds), whereas in kinesin-organized asters, the plus ends were concentrated in the center (*14*). In both kinds of asters, the motors accumulated in the aster center, as revealed by the use of fluorescently labeled motor complexes.

We then investigated whether structures with new topologies could form by mixing the two motor complexes of opposite polarity (Fig. 2B). We started with low motor concentrations corresponding to the regime in which kinesin alone would form MT vortices and Ncd alone would form small MT asters. This resulted in the assembly of a pattern containing Ncd asters and kinesin vortices. Increasing the total motor/tubulin ratio without changing the motor/motor ratio led to local alignment of MTs and, at higher ratios, to a network of poles connected by aligned MTs. The network formed when the kinesin/Ncd ratio was about 0.3. If this ratio was decreased or increased by about 30%, one of the motors won the competition, resulting in the generation of either Ncd or kinesin asters.

Using labeled kinesin complexes, we found that kinesin localized to every second "pole" of the network (Fig. 2B). Thus, the MTs were uniformly oriented in the structures, with one pole made of minus ends and the other of plus ends. Plus- and minus-end poles alternated throughout the network, and the MT ends touched each other in a minus-minus or plus-plus manner. The network contained no antiparallel MT overlaps.

To explore how the physical properties of motors and microtubules determine the generation of asters, vortices, and networks, we performed numerical computer simulations (*15*–*17*). We modeled the motor complexes as two identical motors, which could be bound to one or two MTs or diffuse freely in solution (Fig. 3A). Motors bind and unbind stochastically from MTs and move along them in a force-dependent manner. Upon reaching the MT end, motors detach with a finite off-rate $p_{off,end}$. Motor complexes bound to two MTs exert a force on the MTs, causing them to move. This is the ultimate reason for self-organization in this system. MTs are in a state of growth, but approach a finite length owing to subunit depletion. Because of the stochastic nature of the model, structural details are not fully determined by the initial conditions of a simulation—e.g., the exact number of MTs per self-organized aster can vary. But in most cases, the characteristic features of the generated steady-state patterns arise in a deterministic manner, just as in the experiments. We can compare meaningfully the predictions of the theoretical model with experimental results because of the minimal composition of our experimental system. The present biophysical characterization of its components provides most of the model parameters.

We first examined the effect of motor concentration on aster formation by performing simulations, using the kinetic parameter set for kinesin at various motor densities [because simulations are two-dimensional (2D), 3D concentrations are replaced by 2D densities]. Although at very low density no ordered structures emerged, asters formed at higher motor densities (Fig. 3B). Increasing the motor density led to an increase in the incorporation of MTs into the generated asters, i.e., to an increase in the "intensity of aster formation." Decreasing the processivity (v/p_{off})—i.e., the average distance a motor moves along a MT before detaching—reduced the intensity of aster formation at all motor densities (Fig. 3C) (*18*). An increase in motor density could—within limits—compensate for a decreased processivity. Kinetic parameters could also compensate for changes in other kinetic parameters. This explains why motor constructs with different kinetic properties, like kinesin and Ncd, can generate similar asters in our in vitro system. Changing the motor density, speed (v), and unbinding rate (p_{off}) did not induce a transition from aster to vortex, i.e., did not affect the topology of the self-organized structures.

In addition to these quantitative chang-

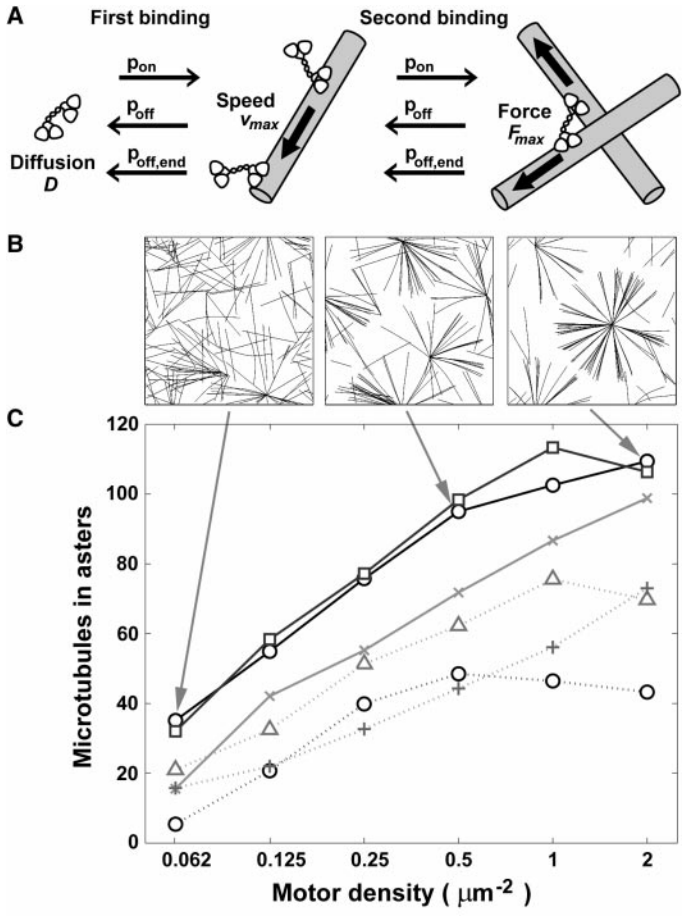

Fig. 3. Numerical computer simulations. (**A**) Schematic representation of the model used for the simulations. Unless otherwise stated, simulations were performed with kinesin-like parameters: binding rate $p_{on} = 50\ s^{-1}$, unbinding rate $p_{off} = 0.5\ s^{-1}$, maximum speed $V_{max} = 1\ \mu m\ s^{-1}$, maximum force $F_{max} = 5$ pN, diffusion coefficient $D = 20\ \mu m^2\ s^{-1}$. For other parameters and the details of the model and the numerical simulations, see (*16*, *17*) and supplementary material (*15*). (**B**) Effect of the motor density on the intensity of aster organization by one kind of motor complex. Asters generated by simulations in a periodic box of 50 μm by 50 μm with an average MT density of 0.05 μm^{-2} and average motor densities M of 0.05, 0.5, and 2.0 μm^{-2} (125 MTs and 125, 1250, and 5000 motors, respectively). The unbinding rate from MT ends was $p_{off,end} = 2.5\ s^{-1}$. (**C**) Variation of kinetic parameters. The total average number of MTs in the three largest asters characterizes the intensity of aster organization and is plotted as a function of the motor density. The simulated time was 500 s. Parameter sets [V (s^{-1}), P_{off} (s^{-1}), and $P_{off,end}$ (s^{-1})] are as follows: (○—○) 1, 0.5, 2.5; (□) 1, 1, 2.5; (×) 1, 5, 2.5; (○···○) 0.2, 0.5, 2.5; (△) 0.2, 0.5, 0.5; (+) 0.2, 0.5, 0.05.

es, some parameter variations also caused qualitative transitions between structures of different topologies. Increasing $p_{off,end}$ to 70 s^{-1} or more (i.e., decreasing the average motor residence time at MT ends to 15 ms or less in the background of kinesin-like parameters) induced the formation of vortices (Fig. 4A). We did not observe a vortex-to-aster transition in simulations by changing the value of another parameter and keeping $p_{off,end}$ constant [for a comparison of this result with experimental results, see (*19*)]. Thus, the residence time at MT ends plays a crucial role with regard to the capacity of motors to focus MTs to a pole (because motor links between MT ends and other MTs can eventually bring MT ends together, if these links are stable). The residence time has not yet been determined for any motor protein. However, in our experimental system, $p_{off,end}$ appears to be higher for the kinesin construct than for the Ncd construct (*18*), because kinesin, in contrast to Ncd, is capable of forming vortices.

We performed simulations of 1:1 mixtures of two motors with identical kinesin-like properties but with opposite directionalities. At high motor densities, when each of the individual motors alone formed asters, a mixture of two such motors generated an irregular network of connected poles (Fig. 4B) similar to the one observed in the experiment (Fig. 2B). Decreasing the motor density from 0.5 to 0.03 μm^{-2} in such a mixture caused the generation of isolated asters of both polarities (Fig. 4C). We then studied a 1:1 mixture of an aster-forming motor complex (long residence time at MT ends) and a vortex-forming motor complex (short residence time at MT ends) with opposite directionality of movement. At low motor densities, mixtures of asters and vortices did form, whereas at higher motor densities asters of one polarity were formed by one of the motors, while the other one induced the formation of curved MT bundles between these asters (Fig. 4C). Networks of connected poles did not form [for a comparison of these simulation results with experimental results, see (*19*)]. This demonstrates that the formation of these networks is also sensitive to the residence time of the motors at MT ends (i.e., to $p_{off,end}$). We also simulated mixtures of motors with different kinetic parameters and found that they would form networks at a given density, as long as both motors could, on their own at this density, organize all MTs into asters.

The MT structures classically found in cells are asters, bundles, spindles, or more complex architectures found in protozoa (*20*). From the results of our simulations, we predict that the motor that forms asters in vivo, dynein (*21*), should form processive oligomers that have a long residence time at MT ends, emphasizing the importance of motor-MT interactions at MT ends (*22*, *23*). The other structures observed in this study, vortices and networks, do not seem to have counterparts in the living world. Yet, in the networks formed by two motors, the two oppositely oriented sets of parallel aligned MTs are reminiscent of the two half-spindles in a bipolar mitotic spindle. There are important differences, however. In the network, both MTs and motors are entirely sorted. In the mitotic spindle midzone, MTs

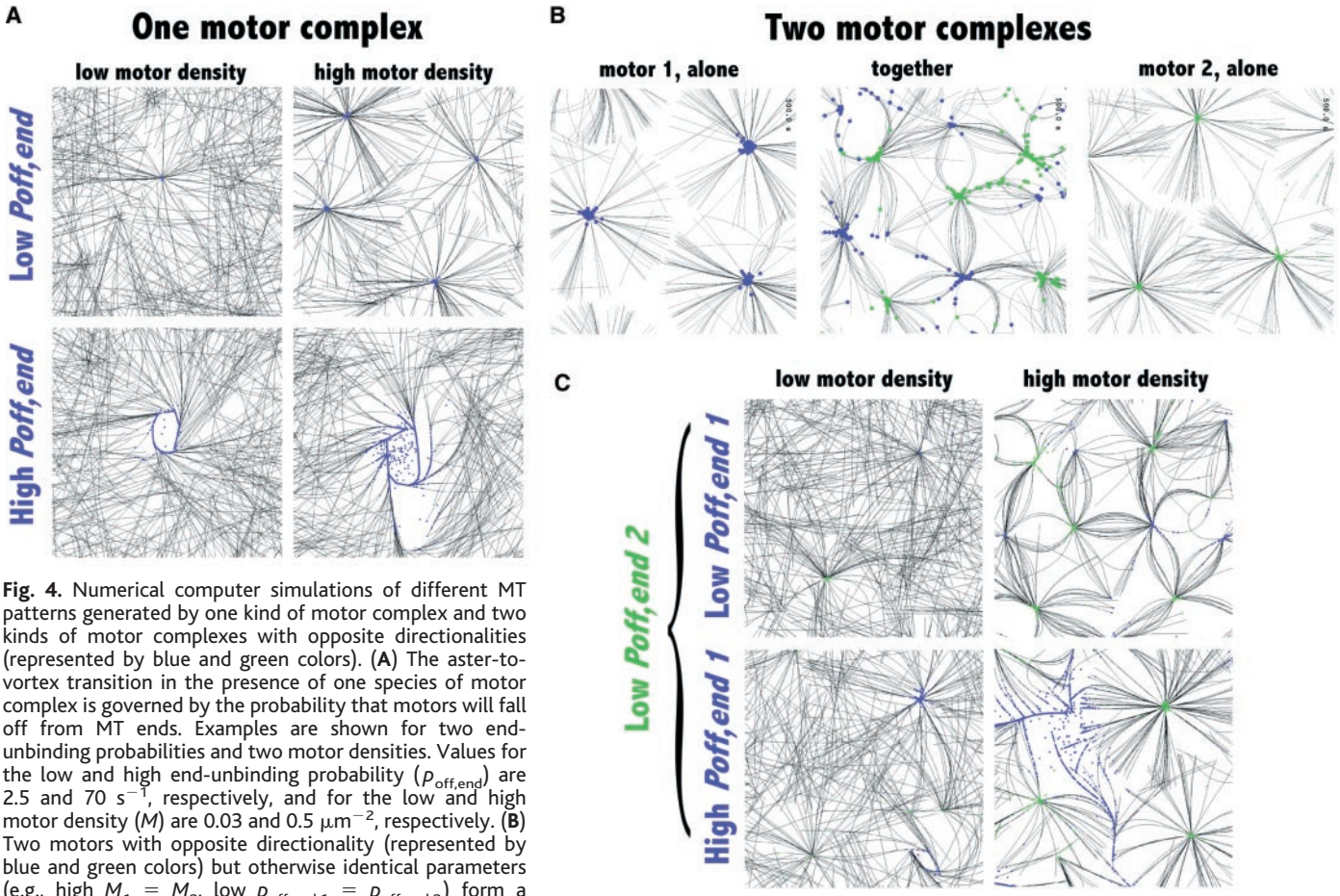

Fig. 4. Numerical computer simulations of different MT patterns generated by one kind of motor complex and two kinds of motor complexes with opposite directionalities (represented by blue and green colors). (**A**) The aster-to-vortex transition in the presence of one species of motor complex is governed by the probability that motors will fall off from MT ends. Examples are shown for two end-unbinding probabilities and two motor densities. Values for the low and high end-unbinding probability ($p_{off,end}$) are 2.5 and 70 s^{-1}, respectively, and for the low and high motor density (M) are 0.03 and 0.5 μm^{-2}, respectively. (**B**) Two motors with opposite directionality (represented by blue and green colors) but otherwise identical parameters (e.g., high $M_1 = M_2$, low $p_{off,end,1} = p_{off,end,2}$) form a network of poles connected by aligned MTs. (**C**) Patterns generated by mixtures of two species of motors with opposite directionalities and identical, low off-rates from MT ends (low $p_{off,end,1} = p_{off,end,2}$) (top) or with one low and one high off-rate from MT ends ($p_{off,end,1} \neq p_{off,end,2}$) (bottom). Both cases are shown for low and high motor densities ($M_1 = M_2$). The size of the periodic box is 100 μm by 100 μm, of which 60% are shown. The simulated time is 1500 s [or 500 s for the simulation with $p_{off,end} = 2.5\ s^{-1}$ and $M = 0.5\ \mu m^{-2}$ in (A), because these asters form more rapidly than the other structures]. For all other parameters, see supplementary material (*15*).

form stable antiparallel overlaps in which motors are present (*24–26*). It will be interesting to determine which properties are responsible for the stabilization of such antiparallel MT overlaps.

In exploring the generic steady-state patterns that could emerge from mixtures of MTs and one or two oligomeric motors of opposite directionality, we have found a limited number of patterns: radial MT structures, either asters or vortices, or networks of poles connected by aligned MTs. Using computer simulations, we found that changes in the value of many parameters did not affect the topology of the pattern, whereas changes in other parameter values did. Those parameters are potential key targets for regulation. Many complex biological structures are also collective out-of-equilibrium assemblies. In the past, they have been described mainly by attributing qualitative "functions" to some of their constituent molecules. Here, we have used kinetic parameters describing the properties and interactions of the molecules to deduce the structures produced by the ensemble.

References and Notes

1. H. Fraenkel-Conrat, R. C. Williams, *Proc. Natl. Acad. Sci. U.S.A.* **41**, 690 (1955).
2. S. Inoue, in *40th Symposium of the Society for Developmental Biologists*, S. Subtelny, P. B. Green, Eds. (Liss, New York, 1982), pp. 30–35.
3. A. M. Turing, *Philos. Trans. R. Soc. London Ser. B* **237**, 37 (1952).
4. I. Prigogine, G. Nicolis, *J. Chem. Phys* **46**, 3542 (1967).
5. B. L. Goode, D. G. Drubin, G. Barnes, *Curr. Opin. Cell Biol.* **12**, 63 (2000).
6. S. L. Rogers, V. I. Gelfand, *Curr. Opin. Cell Biol.* **12**, 57 (2000).
7. W. Saunders, V. Lengyel, M. A. Hoyt, *Mol. Biol. Cell* **8**, 1025 (1997).
8. C. E. Walczak, I. Vernos, T. J. Mitchison, E. Karsenti, R. A. Heald, *Curr. Biol.* **8**, 903 (1998).
9. D. J. Sharp *et al.*, *Mol. Biol. Cell* **11**, 241 (2000).
10. F. Nédélec, T. Surrey, A. C. Maggs, S. Leibler, *Nature* **389**, 305 (1997).
11. R. J. Stewart, J. P. Thaler, L. S. Goldstein, *Proc. Natl. Acad. Sci. U.S.A.* **90**, 5209 (1993).
12. The kinesin construct contains the NH_2-terminal 401 amino acids of *Drosophila* kinesin and a COOH-terminal biotinylation domain (*27*). GST-Ncd consists of the COOH-terminal 506 amino acids of *Drosophila* Ncd fused to an NH_2-terminal GST tag (*11*). Both proteins were expressed in bacteria and purified as described (*28*). The motors were flash-frozen in liquid ethane and stored in liquid nitrogen. Fluorescein-labeled streptavidin was from Molecular Probes, monoclonal anti-GST was purified from mouse ascites (Sigma), and tubulin was purified from cow brain. Oligomeric motor complexes were made immediately before the experiment by mixing biotinylated kinesin and streptavidin or GST-Ncd and anti-GST, resulting in complexes of 8 (*10*) or 8 to 12 motors, respectively. For the size determination of Ncd complexes by gel filtration, ultracentrifugation, and fluorescence correlation spectroscopy, and for the preparation of polarity-marked MT seeds, see supplementary material (*15*). Self-organization experiments were performed essentially as described (*10*, *28*), with agarose and bovine serum albumin–coated glass cover slips for microscopy to avoid motor-mediated gliding of MTs on the glass surface. Final buffer concentrations in experiments with Ncd complexes and kinesin complexes were typically 800 mM glycerol, 140 mM glutamate, 20 mM Pipes, 12.5 mM imidazole, 12.5 mM KCl, 4.0 mM $MgCl_2$, 0.5 mM EGTA, 3.0 mM ATP, 1.4 mM GTP, 2.5 mM phosphoenolpyruvate, pyruvate kinase (350 U ml^{-1}; Sigma, P-7768) (pH 6.9), 1.0 mM mercaptoethanol, 0.15 mM dithiothreitol, and 2.6 μM paclitaxel (Molecular Probes). [For a discussion of the effect of paclitaxel on self-organization, see supplementary material (*15*).] Final concentrations in experiments with one motor complex were similar to those with two motors [for details, see (*28*)]. Immediately after the final mixing steps, samples of 1.3 μl were warmed on the microscope to 30°C (to start MT polymerization), maintained at this temperature throughout the experiment, and observed by dark-field and fluorescence microscopy on a Zeiss Axiovert 10 with a digital image recording system (Sony SSC M370CE charge-coupled device, Power Mac G3 and Scion Image 1.62).
13. The structures shown in Fig. 2A were stable for at least 1 hour, then protein aggregation started to become visible. We also confirmed by simulations that vortices and asters are stable for at least 1 hour.
14. F. Nédélec, T. Surrey, A. C. Maggs, *Phys. Rev. Lett.* **86**, 3192 (2001).
15. Supplementary data are available on *Science* Online at www.sciencemag.org/cgi/content/full/292/5519/1167/DC1 and at www.embl-heidelberg.de/ExternalInfo/karsenti/self.
16. F. Nédélec, thesis, Université Paris XI, Orsay (1998).
17. _____, in preparation.
18. When the processivity was reduced to one step before unbinding, asters stopped forming, and this could no longer be compensated in the range of parameter variations studied here. Indeed, this result suggests that the oligomeric Ncd complex used in the experiments is considerably processive—in contrast to dimeric Ncd, which is not (*29*). However, small numbers of Ncd molecules, when acting cooperatively, can be processive (*30*). This is probably the case for our construct, which consists of 8 to 12 Ncds (*15*). Similarly, this might also explain why $p_{off,end}$ of the Ncd complex appears to be low.
19. It is surprising that in experiments with kinesin, the formation of asters as compared with vortices is observed when the kinesin concentration is changed (Fig. 2A), whereas in simulations, this transition in response to a change in density only is not observed (Fig. 4A). This discrepancy could be due to the increase in effective residence time at MT ends of kinesin complexes with increasing motor concentration. This concentration dependence could arise from crowding and aggregation effects that occur when the motors become strongly locally concentrated (Figs. 1 and 2). Such a dependence between parameters is not accounted for in the minimal model used for the simulations. We saw the same behavior of kinesin in experiments where both motors—kinesin and Ncd—were present. The networks transformed to a mixture of Ncd asters and kinesin vortices when the motor/MT ratio was decreased, whereas in simulations the network transformed to a mixture of asters of opposite polarity. Again, this can be explained by assuming that kinesin's off-rate from MT ends is concentration-dependent. These results indicate that the experimentally observed transitions in Fig. 2A from b to c, and in Fig. 2B from a to c, correspond to simulated transitions in Fig. 4, A and C, from bottom left to top right.
20. M. Sleigh, *The Biology of Protozoa* (Arnold, London, 1973).
21. R. Heald *et al.*, *Nature* **382**, 420 (1996).
22. T. J. Mitchison, *Philos. Trans. R. Soc. London Ser. B* **336**, 99 (1992).
23. A. A. Hyman, E. Karsenti, *Cell* **84**, 401 (1996).
24. N. R. Barton, A. J. Pereira, L. S. Goldstein, *Mol. Biol. Cell.* **6**, 1563 (1995).
25. K. E. Sawin, T. J.Mitchison, *Proc. Natl. Acad. Sci. U.S.A.* **92**, 4289 (1995).
26. D. J. Sharp *et al.*, *J. Cell Biol.* **144**, 125 (1999).
27. T. Surrey *et al.*, *Proc. Natl. Acad. Sci. U.S.A.* **95**, 4293 (1998).
28. F. Nédélec, T. Surrey, *Methods Mol. Biol.* **165**, 213 (2000).
29. I. M. Crevel, A. Lockhart, R. A. Cross, *J. Mol. Biol.* **273**, 160 (1997).
30. M. J. deCastro, C. H. Ho, R. J. Stewart, *Biochemistry* **38**, 5076 (1999).

31. We thank L. S. Goldstein for the GST-N195 plasmid; A. J. Ashford, A. Desai, R. Tournebize, and H. Wilhelm for unlabeled and labeled tubulins; D. N. Drechsel and M. Groves for help with the size determination of the Ncd complex; and A. C. Maggs for help with the simulations.

12 February 2001; accepted 23 March 2001

Pot1, the Putative Telomere End-Binding Protein in Fission Yeast and Humans

Peter Baumann and Thomas R. Cech*

Telomere proteins from ciliated protozoa bind to the single-stranded G-rich DNA extensions at the ends of macronuclear chromosomes. We have now identified homologous proteins in fission yeast and in humans. These Pot1 (protection of telomeres) proteins each bind the G-rich strand of their own telomeric repeat sequence, consistent with a direct role in protecting chromosome ends. Deletion of the fission yeast *pot1*$^+$ gene has an immediate effect on chromosome stability, causing rapid loss of telomeric DNA and chromosome circularization. It now appears that the protein that caps the ends of chromosomes is widely dispersed throughout the eukaryotic kingdom.

Telomeres, the protein-DNA complexes at chromosome ends, protect chromosomes from degradation and end-to-end fusion, and they serve as substrates for extension by telomerase. The telomeric DNA terminates with a single-stranded overhang of the G-rich strand in ciliated protozoa (*1*), yeast (*2, 3*), and mammalian cells (*4–6*). In budding yeast, the Cdc13 protein binds to this single-stranded DNA, protecting the chromosome end (*7, 8*) and recruiting telomerase (*9*). In the hypotrichous ciliate *Oxytricha nova*, an α-β protein heterodimer

Howard Hughes Medical Institute, Department of Chemistry and Biochemistry, University of Colorado, Boulder, CO 80309, USA.

*To whom correspondence should be addressed. E-mail: thomas.cech@colorado.edu